electronics

MDPI

Article

# Implementation of Constant Temperature–Constant Voltage Charging Method with Energy Loss Minimization for Lithium-Ion Batteries

**Guan-Jhu Chen [1], Chun-Liang Liu [2,*], Yi-Hua Liu [3] and Jhih-Jhong Wang [3]**

1 Department of Electronic Engineering, National Chin-Yi University of Technology, Taichung 411030, Taiwan; gjchen@ncut.edu.tw
2 Department of Electrical Engineering, National Yunlin University of Science and Technology, Yunlin 640301, Taiwan
3 Department of Electrical Engineering, National Taiwan University of Science and Technology, Taipei 106335, Taiwan; yhliu@mail.ntust.edu.tw (Y.-H.L.); m11007c02@mail.ntust.edu.tw (J.-J.W.)
* Correspondence: clliu@yuntech.edu.tw

**Abstract:** Effective charging techniques must consider factors such as charging efficiency, lifecycle, charging time (**CT**), and battery temperature. Currently, most charging strategies primarily focus on **CT** and charging losses (**CL**), overlooking the crucial influence of battery temperature on battery life. Therefore, this study proposes a constant temperature–constant voltage (**CT**-CV) charging method based on minimizing energy losses. The charging process is primarily divided into three stages. In the first stage, a constant current (CC) charging is implemented using a 2C rate that aims to expedite battery charging but may result in a rapid temperature increase. The second stage involves constant temperature charging, where the charging current is regulated based on battery temperature feedback using a PID controller to maintain a stable battery temperature. The third stage is constant voltage (CV) charging, where a fixed current is applied continuously until the current drops below the charging cutoff current. After completion of the charging process, the charging time can be calculated, and charging losses can be determined by incorporating the battery equivalent circuit model (ECM). To determine the optimal transition time, the paper employs Coulomb counting and the battery ECM, considering both **CT** and losses to simulate the transition time with minimal **CL**. This approach achieves optimization of transition points by establishing ECM, measuring internal impedance of the battery, and simulating various charging scenarios, and eliminates the need for multiple actual experiments. Experimental results show that the charging time (**CT**) should be reduced and the maximum temperature rise (**TR**) should be reduced under the same average **TR** condition of the proposed method. At the same **CT**, the average **TR** and the maximum **TR** should both decrease. The charging method proposed in this study exhibits the following advantages: (1) simultaneous consideration of the battery's equivalent circuit model and charging time; (2) the achieved transition point demonstrates characteristics of minimized charging losses; (3) eliminates the need for multiple experimental iterations.

**Keywords:** lithium-ion battery; equivalent circuit model; constant temperature–constant voltage charging method (CT-CV); minimizing charging losses (**CL**)

check for updates

**Citation:** Chen, G.-J.; Liu, C.-L.; Liu, Y.-H.; Wang, J.-J. Implementation of Constant Temperature–Constant Voltage Charging Method with Energy Loss Minimization for Lithium-Ion Batteries. *Electronics* **2024**, *13*, 645. https://doi.org/10.3390/electronics13030645

Academic Editor: Fabio Corti

Received: 29 December 2023
Revised: 26 January 2024
Accepted: 30 January 2024
Published: 4 February 2024



## 1. Introduction

In recent years, due to the global advocacy for green energy, countries worldwide have invested significant resources in the development of renewable energy, energy storage systems, and the electric vehicle industry. This not only ensures a stable energy supply but also reduces the reliance on traditional fossil fuel-based power generation, subsequently decreasing air pollution and greenhouse gas emissions. Li-ion batteries are pivotal due to prolonged lifecycle span and capacity to endure strong power discharges. These characteristics position them as the predominant choice for applications demanding sustained periods of high-energy output, solidifying their status as the mainstream battery in the market.

As the use of lithium-ion batteries continues to grow in stationary and portable electronic devices, charging technology becomes paramount [1–5]. However, addressing key challenges, including shortening charging time (**CT**), reducing battery charging temperature rise (**TR**) generated within a battery during its usage or charging and discharging processes due to internal electrochemical reactions, and improving prolonging battery life, remains a focal point in lithium-ion battery charging technology research. Numerous studies have already been conducted in this area [6–26].

Lithium-ion battery charging algorithms are mainly classified into three categories: constant current–constant voltage (CC-CV) charging, pulse current charging, and multi-stage constant current (MSCC) charging technique. The widely employed approach is CC-CV charging, involving a two-stage process. Initially, the battery undergoes CC charging, followed by CV charging. In the constant current (CC) phase, the battery voltage experiences a gradual increase. When the preset voltage is reached, the charging process transitions to the constant voltage (CV) stage, where the charging current decreases. The charging process is considered finished when the charging current decreases to the minimum value set by the manufacturer, such as 0.02C. Although using a two-stage method reduces implementation costs, it results in a higher average surface temperature of the battery and longer **CT** during the constant voltage stage.

To address the limitations of the CC-CV charging technique, ref. [6] utilizes phase control, employing error as a manipulation command. This output is fed into the current source circuit, generating a corresponding charging current and achieving a profile similar to CC-CV charging [7]. In CC mode, a current pump charging method is used, maintaining a **CT** similar to CC-CV while significantly enhancing efficiency [8]. Utilizing battery open circuit voltage (OCV) and representing the charging current using fuzzy input membership functions produces the charging current as the output and allows for increased energy injection during CV mode [9]. Focusing on the correlation between constant current charge time (CCCT) and constant voltage charge time (CVCT) under a CC-CV profile with Li-ion battery degradation and a novel health indicator, the CV-CC time ratio is introduced for degradation analysis [10]. A grey-predicted Li-ion battery charge system is employed to improve capacity during the CV stage.

For the pulse current (PC) charging method, efforts are made to obtain a larger pulse charging current [11]. Adjustments are made to the pulse frequency [12], and modifications are made to the pulse duty cycle [13,14]. To generate various charging waveform variations, adjustments are made to the pulse current magnitude, pulse width, and pulse rest time. In the pursuit of maximizing charging capacity and efficiency, minimizing **CT**, and reducing charging losses (**CL**), ref. [15] uses Taguchi orthogonal array to find optimal parameters.

The MSCC charging technique involves the utilization of multiple CC parameters for battery charging. The current literature highlights various benefits, such as prolonged lifecycle, improved charging **TR**, high charging efficiency, and enhanced **CT** [13–20]. Determining optimal current parameters for each stage in this method poses challenges, and the two following main approaches are commonly employed for identifying the optimal charging profile (OCP): soft computing techniques and experimental design techniques. Soft computing methods encompass orthogonal arrays [16,17], Taguchi methods [18,19], optimization algorithms [20,21], and computational optimization [22]. To achieve a full SOC of 100%, ref. [23] employs integer linear programming to find the OCP for MSCC, followed by the CV stage after the OCP stages. Ref. [24] employs a Taguchi-based particle swarm optimization algorithm to find an optimal four-stage constant current charge pattern aiming to maximize capacity for prolonged runtimes in the shortest charging time. The objective is to maximize the cost function considering both charging time and discharge capacity ratio [25]. SOC serves as a switching condition in MSCC, and the Taguchi method is employed to identify optimized current values for each stage.

Charging techniques must consider factors such as **TR**, **CT**, and lifecycle. Although various optimization algorithms show promising results, their practical applicability in practical situations may be limited. The recent trend of fast charging, accomplished by elevating currents to reduce times, raises safety concerns regarding heightened battery temperatures. This paper addresses this issue using the CT-CV charging method [26]. By establishing a battery ECM, the parameters of the ECM are measured using AC impedance analysis. Gaussian curve fitting is employed to establish the relationship between different state of charge (SOC) levels and battery model parameters. Subsequently, MATLAB is utilized to simulate a charging process using the 0.5C to 4C constant current–constant voltage (CC-CV) charging method, and simulating **CL** and **CT**, the optimal transition time for modes is determined to minimize losses. During the charging process, a proportional–integral–derivative (PID) controller is integrated to regulate the current in real-time, maintaining the battery temperature at a set level. This approach mitigates the risk of damage from excessively high temperatures, ensuring practical and safe charging.

## 2. Lithium-Ion Battery Model

### *2.1. Lithium-Ion Battery Equivalent Circuit Model (ECM)*

Given the complex composition of lithium-ion batteries, this study utilizes a battery equivalent circuit model to approximate the internal electrochemical characteristics. A precise ECM can more closely match the response of real battery operation, enabling the creation of more efficient charging techniques. Consequently, this contributes to advancements in **CT**, **TR** during charging, and the extension of battery lifespan.

To capture the response of a real battery, this paper employs the ECM illustrated in Figure 1, representing a Thevenin battery model. The battery is conceptualized as a voltage source $V_{Ceq}$ in series with an Ohmic resistor $R_s$ and in parallel with a set of polarization capacitor $C_p$ and polarization resistor $R_p$. Here, $V_{OCV}$ is the open-circuit voltage of the battery and $V_T$ is the terminal voltage of the battery. By incorporating $R_p$ and $C_p$, the model aims to simulate the response of a real battery, closely resembling real-world charging and discharging scenarios.

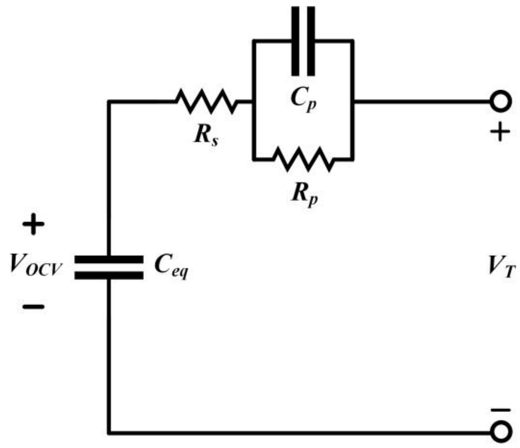


**Figure 1.** Thevenin battery circuit model.

### *2.2. ECM Characteristics*

To examine the electrochemical reaction of the battery across different states and deduce the equivalent impedance of the battery under various conditions, this study employs the method of alternating current impedance analysis to investigate the internal characteristics of the battery. Through this approach, this study aims to measure and acquire the parameters $R_s$, $R_p$, and $C_p$ for the ECM of the lithium-ion battery applied in this study. The forthcoming sections will present the experimental procedures for alternating current impedance analysis.

2.2.1. Introduction to the Selected Battery

The selected battery for this study is the INR-18650-P28A lithium-ion battery introduced by Molicel, as depicted in Figure 2. The battery specifications are elaborated in Table 1.


**Figure 2.** INR-18650-P28A lithium-ion battery.

**Table 1.** INR-18650-P28A lithium-ion specifications [27].

| Molicel INR-18650-P28A Lithium-Ion Battery | |
|---|---|
| Related Capacity | 2800 mAh |
| Minimum Related capacity | 2600 mAh |
| Related Voltage | 3.6 V |
| Standard Charging | CC-CV, 2800 mA |
| Weight | 46 g |
| Suitable Temperature for Charge | 0 °C to 60 °C |
| Suitable Temperature for Discharging | −40 °C to 60 °C |

2.2.2. AC Impedance Analysis

AC impedance analysis involves the application of a low-amplitude AC sinusoidal voltage or current to disturb a battery's positive and negative electrodes. The obtained data encompass current, voltage, and frequency, subsequently converted into AC impedance parameters. This dataset employs the ECM and determines relevant values. When adjusting the input AC frequency, changes in the response curves of real-axis impedance and imaginary-axis impedance can be observed. This graphical representation is commonly called the electrochemical impedance spectrum (EIS).

The Nyquist plot illustrates internal reactions of the battery. Its analysis results, consisting of components such as resistors, inductors, and capacitors, are similar to other response plots with these three components. The response varies depending on the frequency of the applied perturbation. Figure 3 provides a schematic Nyquist plot that illustrates the impedance effects within a battery system.

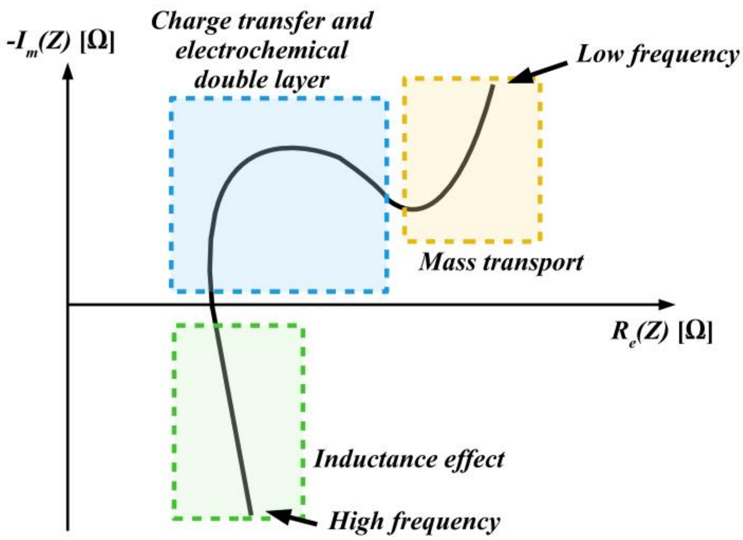


**Figure 3.** Nyquist plot of battery AC impedance effect.

### 2.2.3. Constant Potential Detection for AC Impedance Analysis

When conducting AC impedance measurements, apply a variable-frequency sinusoidal voltage or current signal. In constant voltage mode, the perturbation amplitude should not be too large. Excessive perturbation can disrupt the battery's equilibrium state, leading to measurement distortion.

During the constant potential perturbation detection experiment, the battery responds with a corresponding current due to the perturbation voltage. By detecting the amplitude and phase angle of the current and adjusting and converting signal values, the connection between the perturbation voltage and the corresponding current, considering both magnitude and phase, can be calculated. This process provides the impedance and phase angle. The measurement continues until the specified frequency range is covered. After completing the measurement, the analysis of AC impedance parameters can begin. Figure 4 depicts the flowchart outlining the process of AC impedance analysis.

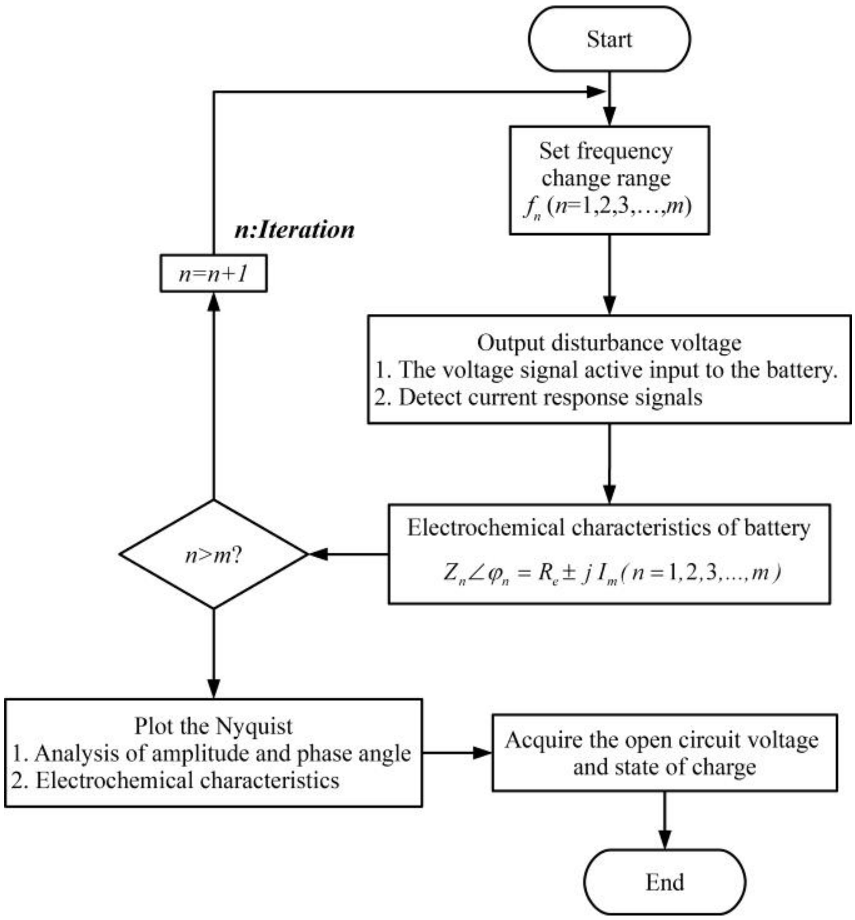


**Figure 4.** AC impedance analysis process.

### 2.2.4. Experimental for AC Impedance Analysis

The AC impedance analyzer utilized is the VSP-300 manufactured by Biologic (Seyssinet-Pariset, France). The battery experiments and result analysis are conducted using EC-Lab V11.30 software. Before measuring AC impedance, ensuring that the remaining capacity of the battery is 100% is crucial. In planning the AC impedance experiment, attention should be paid to adjusting the charge and discharge currents according to the specific battery. For example, in the case of the selected 2.8 Ah lithium-ion battery in this study, a charge or discharge current of 2.8 A represents 1C, indicating that the battery can discharge at 2.8 A for 1 h. The AC impedance of the battery is correlated with its remaining capacity. When conducting measurements, it is crucial to simultaneously consider both the accuracy of the remaining capacity and the required measurement time. In this study, a balance is struck between the accuracy of the battery's ECM and the duration of the measurement. A precision of 1% remaining capacity is chosen for the AC impedance measurement. Before each electrochemical impedance spectroscopy (EIS) test, the battery undergoes a one-hour rest period to attain electrochemical equilibrium, thereby improving the accuracy of the experimental outcomes. The following section will elucidate the experimental settings for AC impedance analysis.

The EC-Lab user interface is illustrated in Figure 5, and the operational steps are divided into five parts:

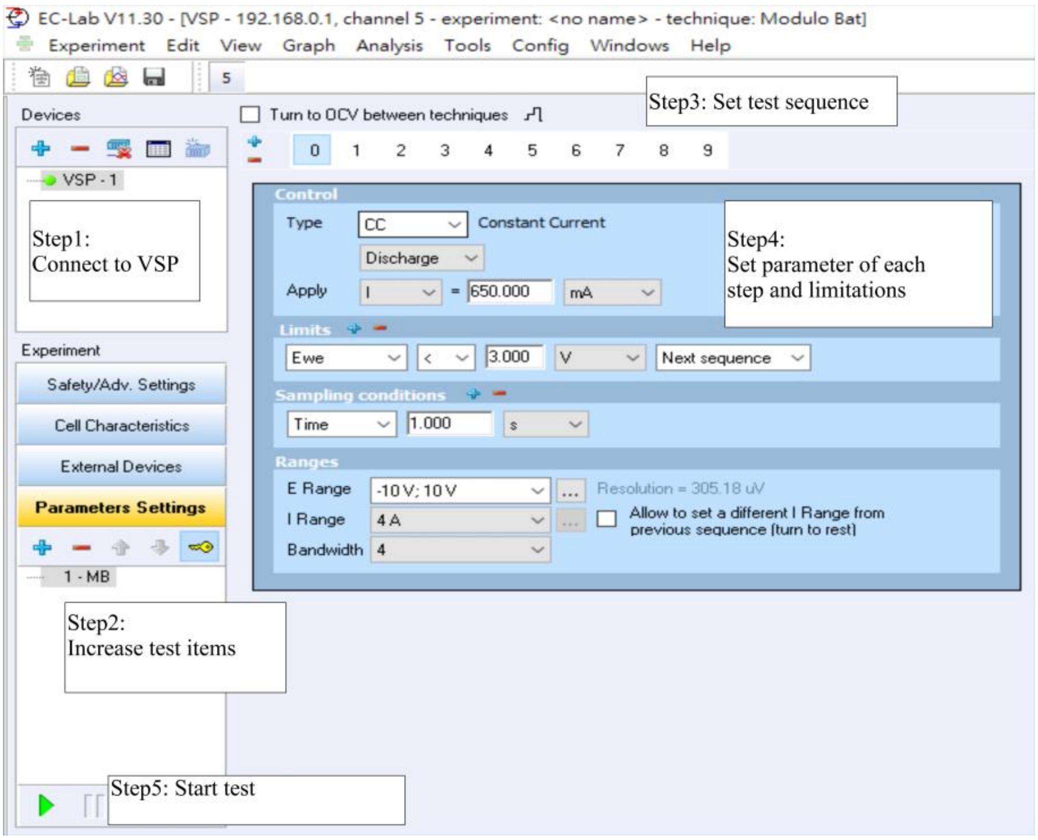


**Figure 5.** EC-Lab user interface.

Step 1: establish a connection between the computer and VSP-300 and confirm the connection is normal.

Step 2: Add a battery test experiment by selecting "Modulo Bat" under the electrochemical techniques list. Modulo Bat provides various battery test experiments, such as constant voltage, constant current, constant power (CP), and electrochemical impedance spectroscopy (EIS).

Step 3: Arrange the experimental procedure. Before starting the experiment, charge the battery to SOC = 100%. During the experiment, discharge the battery to the desired remaining capacity using a constant current and perform AC impedance measurement after allowing the battery to reach electrochemical equilibrium.

Step 4: Set experiment-related parameters. In this study, AC impedance is measured for every 1% remaining capacity. Considering measurement time, the discharge current is set to 0.1 C (0.28 A), estimating an EIS measurement time of approximately 6 min per 1% remaining capacity plus a one-hour rest time. Then, set the constant potential voltage signal with the frequency in the range from 0.1 Hz to 100 kHz and the intervals set at 6 dB, covering most battery operating frequencies. The input voltage amplitude is set to 10 mV to avoid battery damage or induce other electrochemical reactions.

Step 5: commence the AC impedance analysis test.

### 2.2.5. AC Impedance Data Analysis

Following the AC impedance measurement, Nyquist impedance plots can be created for various remaining capacity levels, as depicted in Figure 6. The Z-Fit function in EC-Lab provides different ECMs that can be used to analyze Nyquist impedance plots according to specific requirements. This study employs the Warburg battery equivalent circuit model. The subsequent section offers a comprehensive explanation of the steps involved in analyzing AC impedance, with the operational interface depicted in Figure 7.

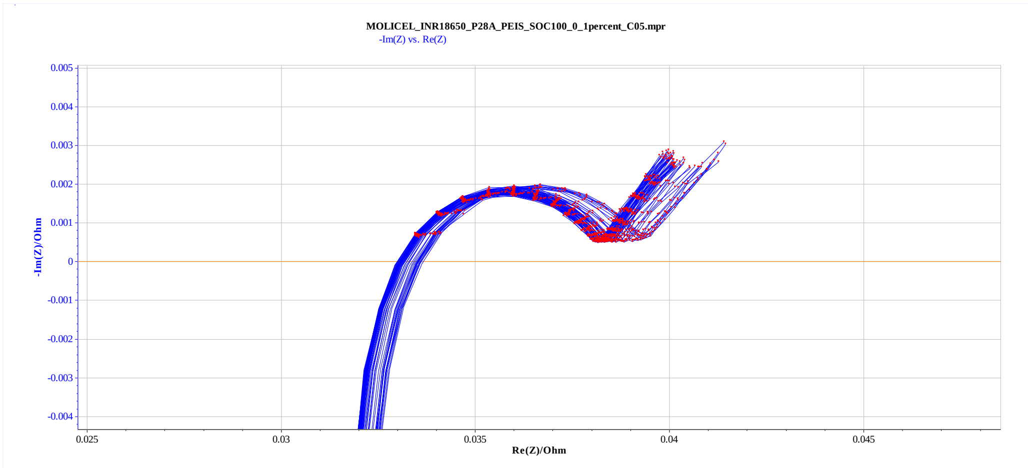


**Figure 6.** Nyquist plots at various SOC levels using EC-Lab (there are 100 sets of data).

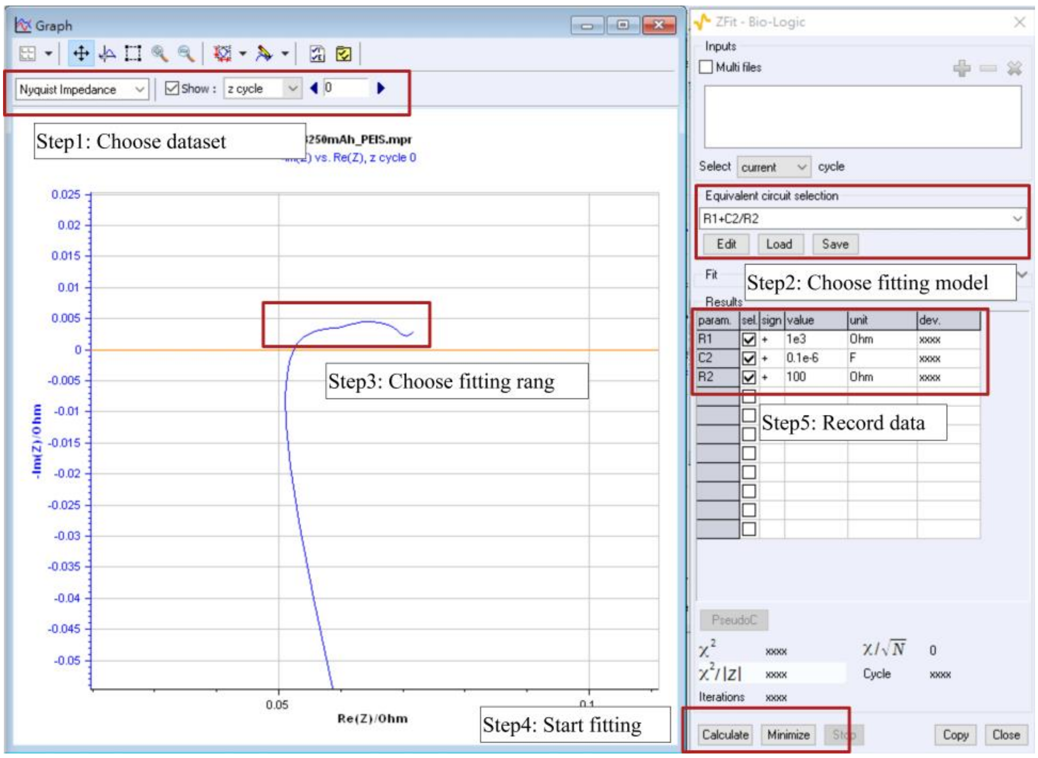


**Figure 7.** AC impedance analysis interface using EC-Lab.

The following introduces the operation steps of the Z-Fit function.

(1) Choose the data presentation method for the measurement, select "Nyquist Impedance" for the Nyquist plot, and choose "z cycle" to show Nyquist plots at various remaining capacity levels.

(2) Z-Fit function is found in "Analysis" option under "Electrochemical Impedance Spectroscopy" within the EC-Lab interface. For this experiment, the chosen model is the ECM. Therefore, select the equivalent model composed of the internal resistance $R_1$, polarization resistance $R_2$, and polarization capacitance $C_2$ for parameter fitting.
(3) The analysis of AC impedance is carried out for each 1% increment in remaining capacity. Begin by selecting the Nyquist plots corresponding to the SOC aspired and subsequently choose the fitting range.
(4) After selecting the fitting range, initiate the curve fitting process by clicking "Minimize" and "Calculate," which will yield the parameters of the fitted curve.
(5) Once the fitted curve parameters are obtained, record them for further analysis.

### 2.3. AC Impedance Characteristics and Fitting

AC impedance provides essential foundational data for constructing equivalent circuit models. In every discharge cycle, the discharge is initiated at 1%, commencing rated capacity for initial experiments. Hence, a total of 101 data points can be obtained, spanning from 100% to 0% capacity. Figure 8 illustrates the relationship curve among $R_s$, $R_p$, and $R_{eq}$ at various SOC levels. The $R_{eq}$ is the sum of $R_s$ and $R_p$. Figure 9 depicts the curve depicting the relationship of the battery OCV at various SOC levels.

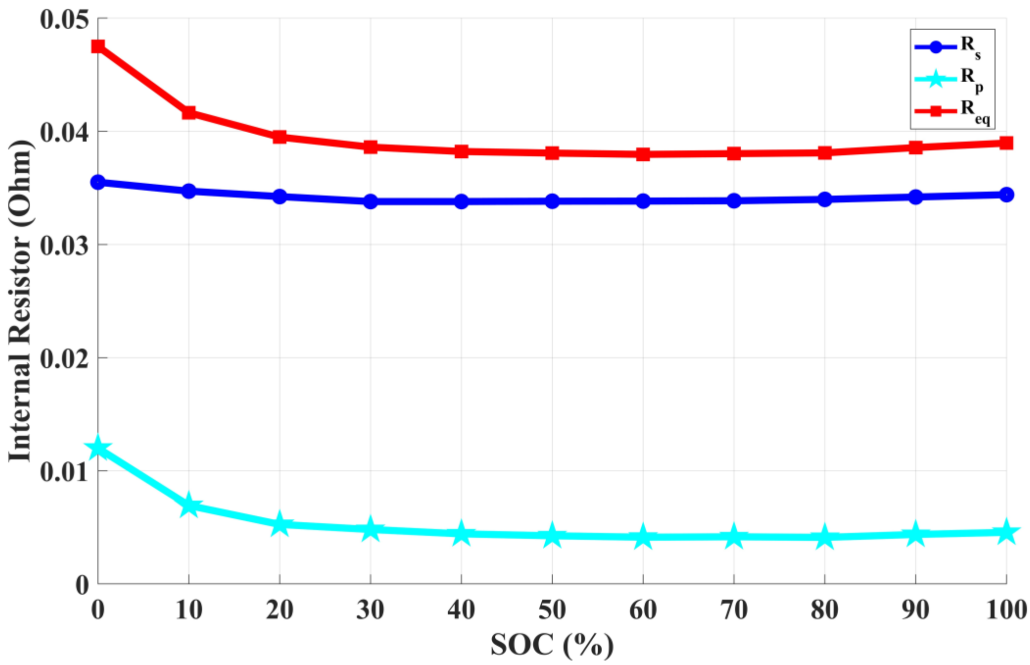


**Figure 8.** Relationship between $R_s$, $R_p$, $R_{eq}$, and SOC.

To simultaneously consider CL and CT while identifying the optimal transition point, it is necessary to take into account the alternating impedance of the battery at various states of charge (SOC). Consequently, this paper imports the measured AC impedance data into MATLAB and utilizes the curve-fitting tool (*cftool*) to be utilized to create curves for fitting remaining capacity and AC impedance. The curve-fitting method in this paper utilizes a Gaussian summation function model, achieves data fitting through nonlinear mapping, and minimizes the loss function. It exhibits good performance in handling complex nonlinear relationship problems, as shown in Equation (1), where Req represents the battery's equivalent impedance, defined as $R_{eq}$ = $R_o$ + $R_p$, and SOC represents the battery's remaining capacity.

The steps to obtain the Gaussian model coefficients are as follows:

(1) Within the Curve Fitter application, proceed to the Curve Fitter tab and access the Data section. Click on "Select Data". In the ensuing "Select Fitting Data" dialog box, designate the X and Y data values.
(2) Navigate to the Curve Fitter tab, and within the Fit Type section, click the arrow to reveal the gallery. Within the fit gallery, choose Custom Equation from the Custom group.
(3) In the Fit Options pane, replace the placeholder text in the equation edit box. "The Gaussian coefficients have a straightforward interpretation, and the exponential background is well-defined".
    a. In the Fit Options pane, proceed to Advanced Options.
    b. In the Coefficient Constraints table within the Advanced Options, adjust the Lower bound to 0, recognizing that peak amplitudes and widths cannot be negative.
    c. Input the StartPoint values as indicated for the specified coefficients.

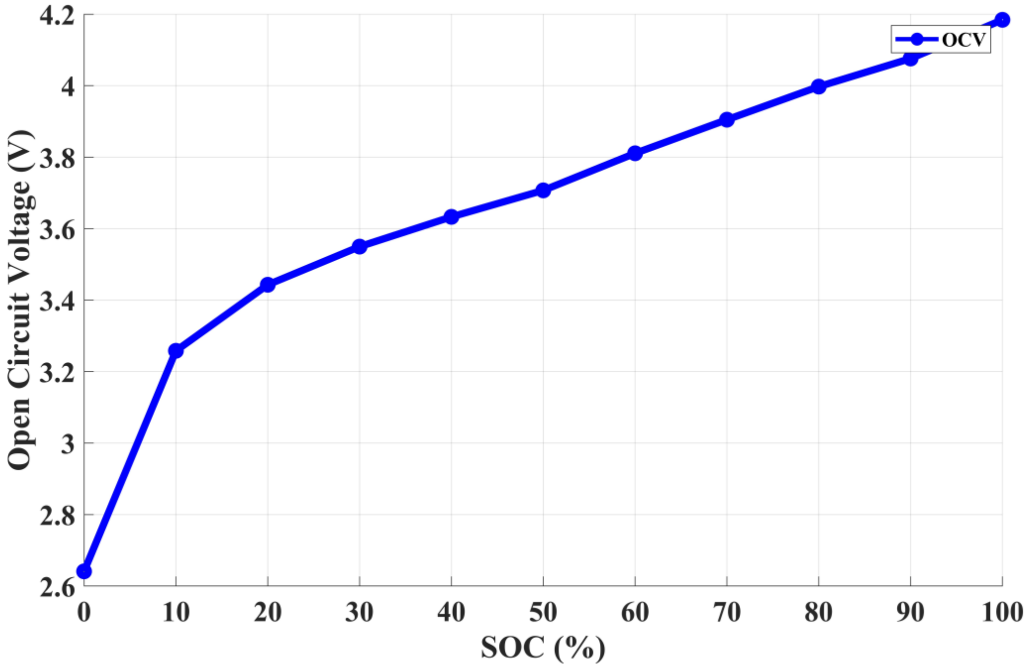


**Figure 9.** Correlation between OCV and SOC.

Table 2 presents the coefficients obtained from the curve fitting. Figure 10 compares the measured impedance with the fitted impedance, while Figure 11 illustrates the error relationship between measured and fitted impedances. The errors obtained in this study are all within 0.014%, validating the application of curve fitting to determine the equivalent impedance at various battery remaining capacities.

$$R_{eq}(SOC) = a_1 \times e^{-\left(\frac{SOC-b_1}{c_1}\right)^2} + a_2 \times e^{-\left(\frac{SOC-b_2}{c_2}\right)^2} + a_3 \times e^{-\left(\frac{SOC-b_3}{c_3}\right)^2} + a_4 \times e^{-\left(\frac{SOC-b_4}{c_4}\right)^2} \quad (1)$$

**Table 2.** Curve fitting coefficient of battery equivalent impedance.

| | | | | | |
|---|---|---|---|---|---|
| $a_1$ | 0.08086 | $b_1$ | −0.6111 | $c_1$ | 0.4565 |
| $a_2$ | 0.07118 | $b_2$ | 9.659 | $c_2$ | 11.19 |
| $a_3$ | 0.0008875 | $b_3$ | 0.2467 | $c_3$ | 0.124 |
| $a_4$ | 0.001624 | $b_4$ | 0.447 | $c_4$ | 0.2168 |

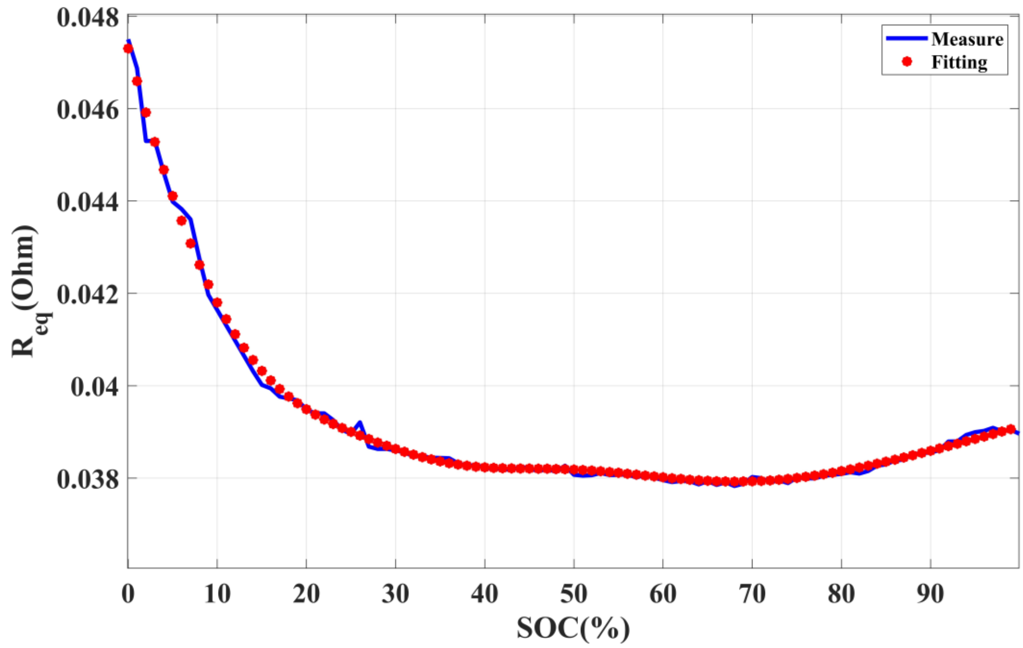


**Figure 10.** Measured impedance and fitting impedance.

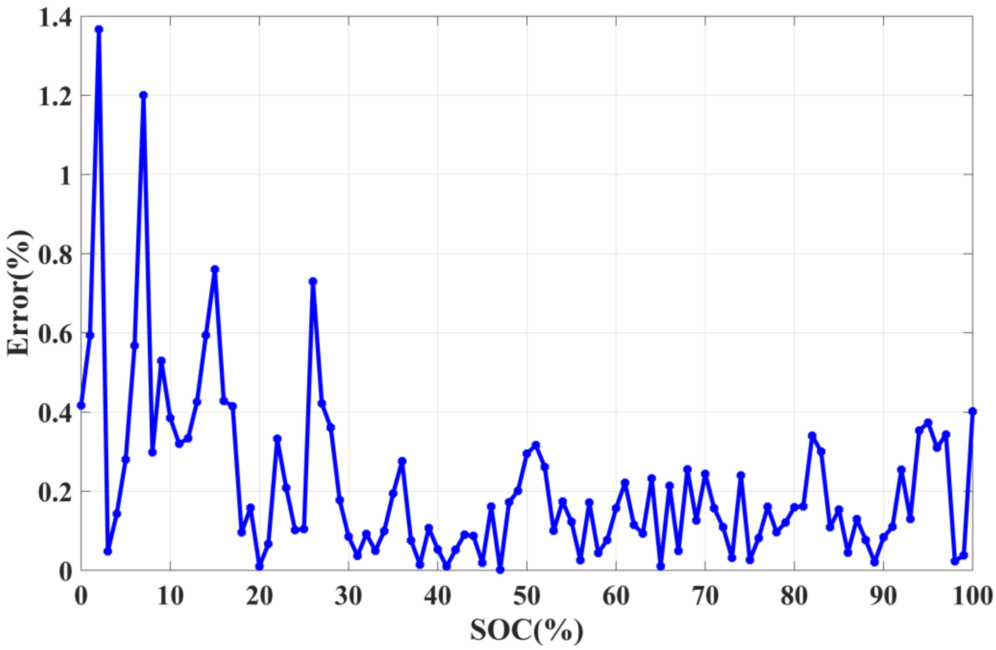


**Figure 11.** Error value of measured impedance and fitted impedance.

## 3. Implementation of Constant Temperature–Constant Voltage Charging for Loss Minimization

This study involves simulating CC-CV charging under various C-rates to identify the minimum and maximum CT and losses. Subsequently, the CT and losses for CT-CV charging are simulated. Taking into consideration both the CT and losses, fitness values are computed for each transition point, aiming to identify the optimal transition points.

### *3.1. CC-CV Charging Method*

The constant current–constant voltage (CC-CV) charging method divides the charging process into two stages. Initially, the battery is charged with a constant current until the battery terminal voltage reaches the rated cutoff voltage. Subsequently, the charging is continued using the cutoff voltage and, at this point, the charging current gradually decreases due to the difference between terminal voltage and internal voltage. When the current drops to the rated cutoff current, it is considered fully charged. This charging method is simple and easy to implement, combining the advantages of both constant current and constant voltage charging methods. However, its drawback is the prolonged charging time [6–9].

### *3.2. CT-CV Charging Method*

CT-CV is an improved charging method based on battery temperature. It utilizes closed-loop control to regulate the charging current. Generally, a higher charging current is required to achieve faster charging of lithium batteries. However, this can lead to increased temperature, and prolonged high-temperature charging accelerates capacity degradation and increases battery impedance [26]. The literature [26] proposes and implements the CT-CV charging technique for lithium-ion batteries. Under the same average TR, CT-CV charging saves 20% of **CT** compared with 1C CC-CV charging. Additionally, under the same **CT**, CT-CV charging reduces the average **TR** by 20% compared with 1C CC-CV charging. This indicates that it is possible to reduce **CT** without compromising battery life due to excessive **TR**. Control of the charging current is necessary to achieve acceptable **TR** at high currents. Figure 12 illustrates the control block of the CT-CV charging method.

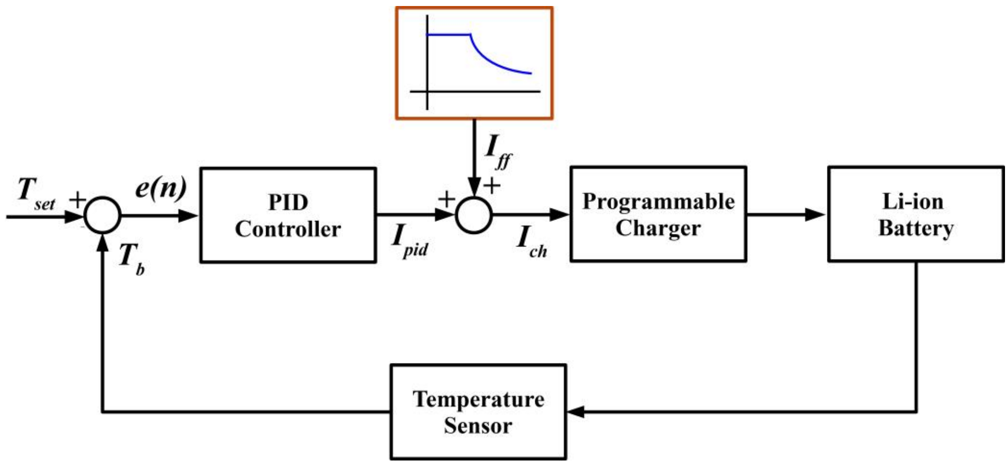


**Figure 12.** The control block of the CT-CV charging technique.

The equations of the PID controller are shown in the following Equations (2)–(6):

$$e(n) = T_{set}(n) - T_b(n) \tag{2}$$

$$I_p(n) = K_p e(n) \tag{3}$$

$$I_i(n) = I_i(n-1) + K_i e(n) \tag{4}$$

$$I_d(n) = K_d[e(n) - e(n-1)] \tag{5}$$

$$I_{pid}(n) = I_p + I_i + I_d \tag{6}$$

The temperature of the battery surface ($T_b$), the set temperature ($T_{set}$), and the temperature error ($e(n)$) are defined in the context. The charging current ($I_{ch}$) is the sum of the feedforward component ($I_{ff}$) and the current adjusted based on the temperature error ($I_{pid}$). As shown in Figure 13, it illustrates the charging current and battery temperature profiles for both the CT-CV and the CC-CV charging method. Table 3 shows the comparison of the CT-CV charging method to the CC-CV charging method.

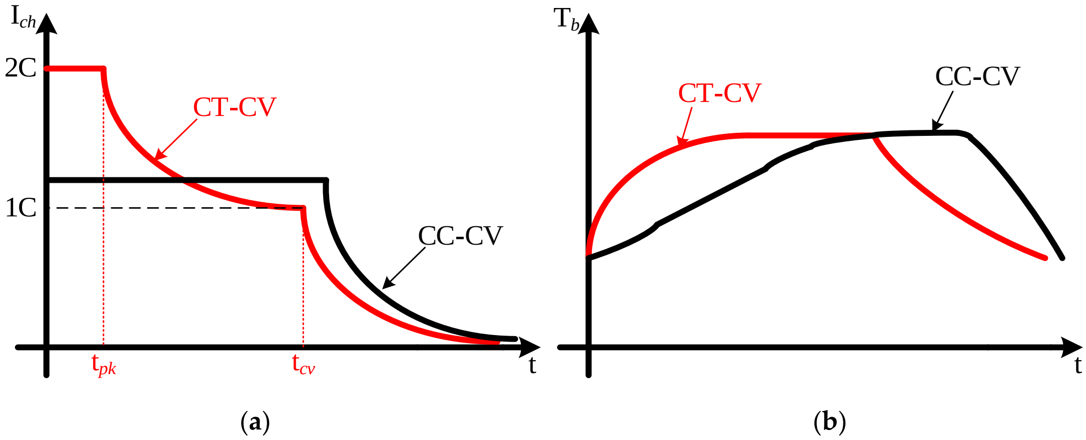


**Figure 13.** Schematic diagrams of (**a**) current profile and (**b**) **TR** for CT-CV and CC-CV.

**Table 3.** Comparison of the CT-CV charging method with the CC-CV charging method.

| | Charging Time (CT) | Charging Loss (CL) | Complexity |
|---|---|---|---|
| CC-CV method | Long | High | Low |
| CT-CV method | Short | Low | High |

In general, the **TR** is relatively slow during the CC phase of CC-CV charging. By increasing the charging current during the CC phase, the battery temperature can quickly reach the preset temperature. Subsequently, the charging current is reduced after reaching the preset temperature to maintain the battery temperature within the desired range. This approach ensures that the highest temperature is equivalent to CC-CV charging. When the battery's remaining capacity exceeds 70%, reducing the charging current helps prevent lithium deposition. Therefore, an exponential decay method is employed, decreasing $I_{ff}$ from 2C to 1C. When the remaining capacity of the lithium battery is low, the internal resistance of the battery is higher. Charging with a higher current at this point would cause the **TR** to increase rapidly to the preset temperature. Figure 14 illustrates the program flowchart for implementing the CT-CV charging method as tested.

### *3.3. The Derivation of the CT-CV Charging Technique Formula*

The method employed in this study to estimate the remaining capacity utilizes Coulomb integration, as shown in Equation (7):

$$SOC(t) = \mathrm{SOC}_0 + \frac{\int_0^t I_{charge}(\tau)\, d\tau}{Q_{rated}} \tag{7}$$

In accordance with Kirchhoff's voltage law, it can be inferred that the sum of the voltage drops across the components in a closed loop is zero. Therefore, the battery terminal voltage $V_T$ can be expressed by Equation (8):

$$V_T = Vc_{eq} + I_{charge} \times R_o + V_p \tag{8}$$

where $V_p$ is the voltage drop across $R_p$ and $C_p$.

The charging duration of the battery can be derived from Equation (7) to obtain Equation (9):

$$\Delta t = \frac{Q_{rated}}{I_{charge}} \times (SOC(t) - \mathrm{SOC}_0) \tag{9}$$

where $SOC_0$ is the initial state of charge before charging, $Q_{rated}$ is the rated capacity of the battery, and $I_{charge}$ is the charging current.

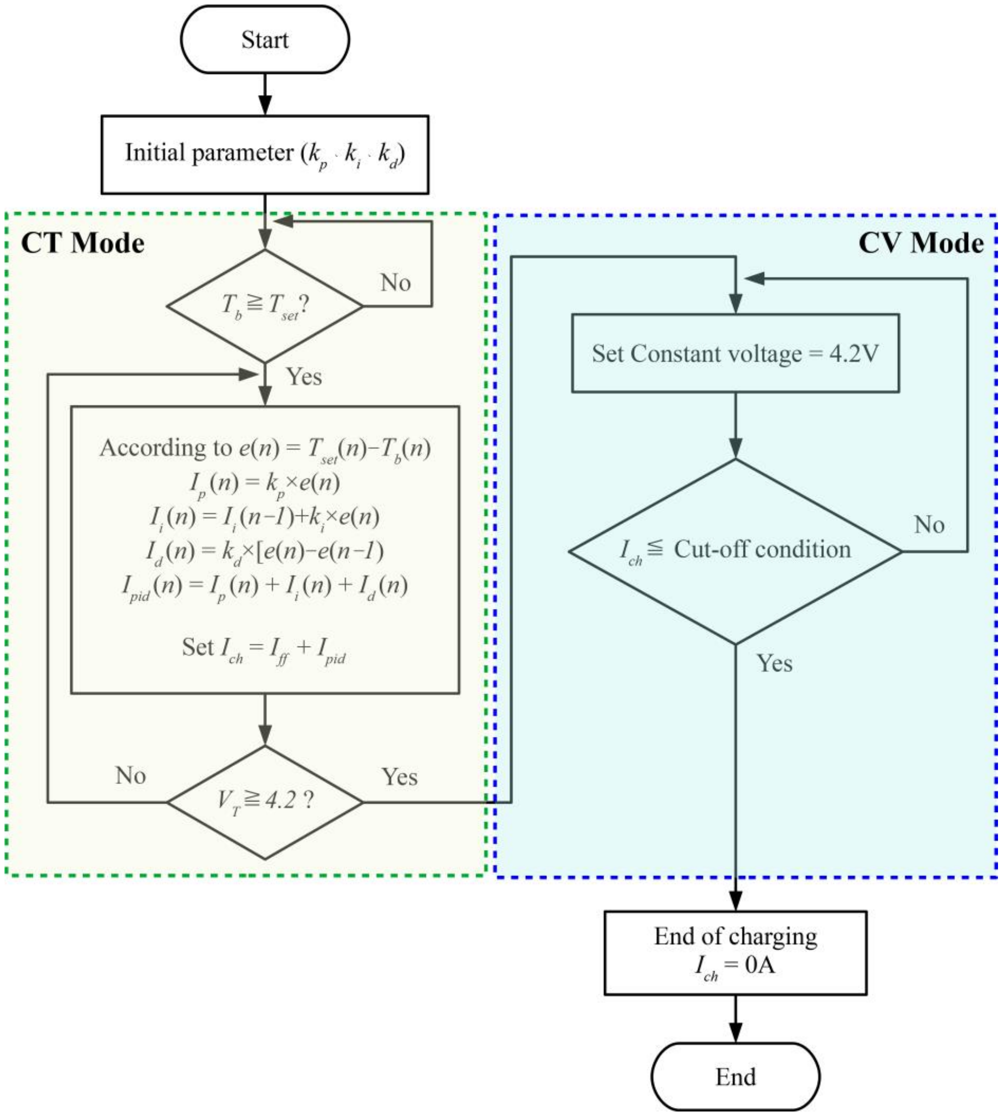


**Figure 14.** The flowchart of implementation of the CT-CV charging technique.

The charging current of the CT-CV charging technique is segmented into three stages: the first stage of CC charging, the second stage of exponential current charging, and the third stage of CV charging. The charging current for each stage can be expressed by Equation (10):

$$I_{charge} = \begin{cases} 2C \quad , \quad 0 \leq t < t_{pk} \\ C \times (1 + e^{-\frac{t - t_{pk}}{\tau}}) \quad , \quad t_{pk} \leq t < t_{cv} \\ (4.2 - V_{ocv})/R_{eq} \quad , \quad t \geq t_{cv} \end{cases} \tag{10}$$

The parameters in the formula include $\tau = t_{pk}$, $V_{ocv}$ and $R_{eq}$ represent the OCV and equivalent resistance of the battery at every 1% remaining capacity, $t_{pk}$ is the duration of the transition to the CV stage, t is the current **CT**, and $t_{cv}$ is the time at which the battery voltage achieves 4.2 V. The charging process ends when the current in the third stage is less than or equal to 50 mA, as specified in the battery's user manual for the termination current.

The **CT** can be obtained from the above equation, and the charging loss L can be simulated and expressed by Formula (11):

$$\Delta L = \int_0^t I_{charge}^2 \times R_{eq}(t)\, dt \tag{11}$$

### 3.4. Fitness Evaluation

The fitness value can be used to confirm whether the found solution is optimal. The optimization method in this paper simultaneously considers both CT and CL as parameters. Hence, this section proposes a method to normalize these two parameters for seamless integration into a fitness value function for performance evaluation. This paper's fitness value evaluation method utilizes the straight-line distance between two points as the score. Figure 15 illustrates the simulation graph of CT and CL for CC-CV charging from a 0.5C rate to a 4C rate. The fitness value is deemed superior if the distance d between the current point ($T_{\_now}$, $L_{\_now}$) and the ideal optimal point ($T_{\_min}$, $L_{\_min}$) is lower. The mathematical expression for the distance $d$ between the two points is given by Equation (12).

$$d = \sqrt{(T_{\_now} - T_{\_min})^2 + (L_{\_now} - L_{\_min})^2} \quad (12)$$

where $L$ is **CL** and $T$ is **CT**. To adjust the weight coefficient between the two parameters, this paper introduces a weighting factor, w = 0.5, and rewrites Equation (12) as Equation (13).

$$Fitness = \sqrt{\alpha \times \left(\frac{T_{\_now} - T_{\_min}}{T_{\_max} - T_{\_min}}\right)^2 + (1-\alpha) \times \left(\frac{L_{\_now} - L_{\_min}}{L_{\_max} - L_{\_min}}\right)^2} \quad (13)$$

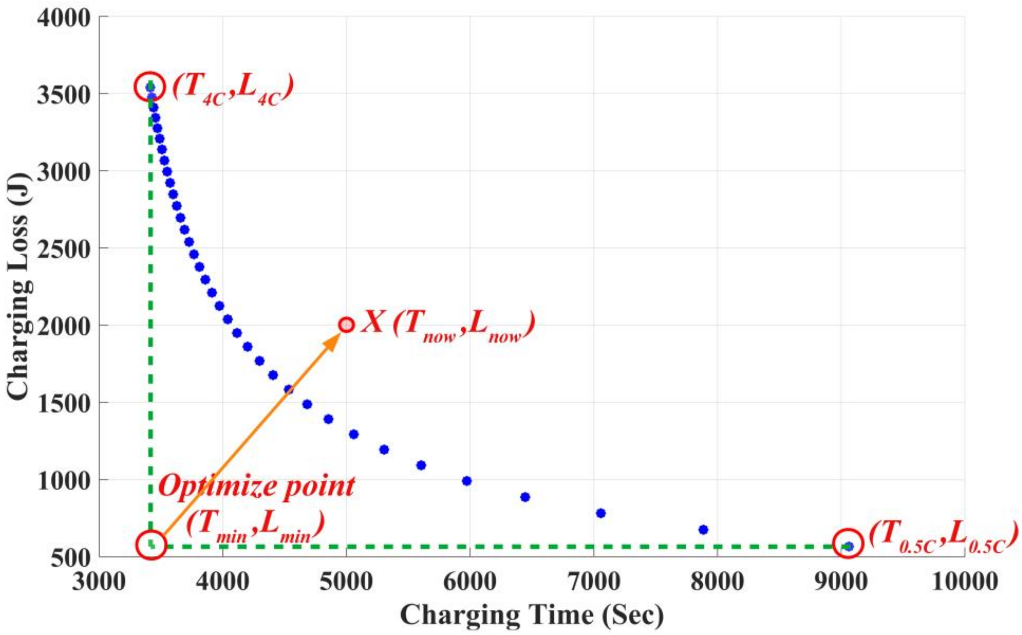


**Figure 15.** Simulation of 0.5C to 4C CC-CV charging method.

## 4. Simulation and Experimental Results

### 4.1. Experimental Setup

The charging equipment used for extended experiments in this study is the PSR 36-7 programmable power supply and human–machine interface produced by GW Instek (New Taipei City, Taiwan). It allows the configuration of various charging modes. The NI-9211 and NI-6009 measurement modules measure battery **TR** and voltage values during battery charging. The battery testing environment is placed inside the Desk-Top DDTH-080-20-BP-43 constant temperature chamber, with the ambient temperature set at 25 °C. Figure 16 depicts the experimental environment setup employed in this study.

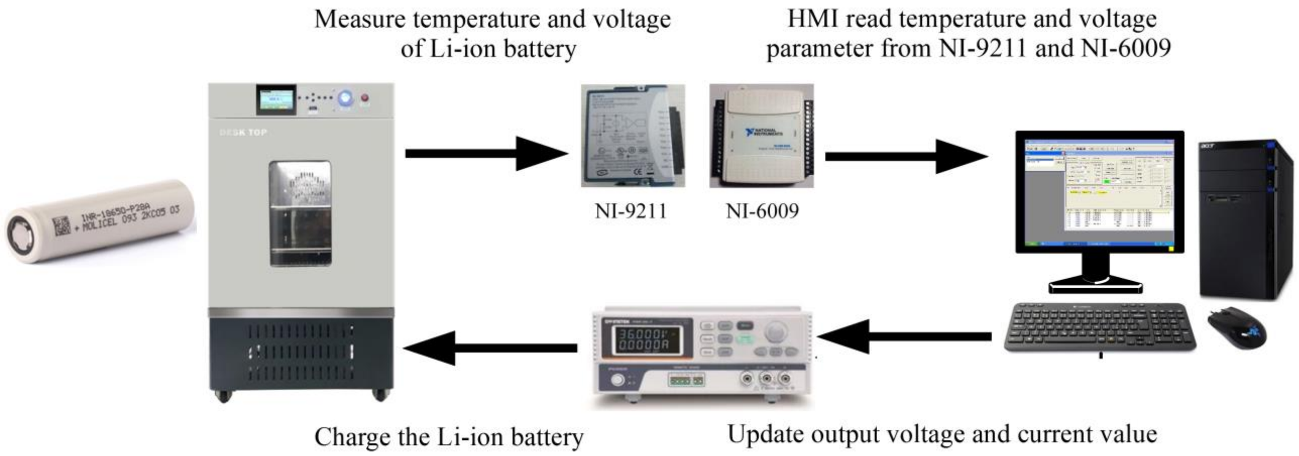


**Figure 16.** Experimental environment setup.

### *4.2. Simulation Results for Minimizing Charging Loss*

As shown in Figure 17, the adaptation value curves for different transition times in the basic CT-CV charging method are depicted. The calculated fitness values based on Equation (13) range from 267 s to 296 s, all approximately equal to 0.2861. Among them, the fitness value at 282 s is the lowest (0.286101). Therefore, this study will compare these three sets to demonstrate that the simulation yields the best-adapted solution, as indicated by the lowest adaptation value. Table 4 presents the simulation results for **CL** and **CT** after 0.5C and 4C CC-CV charging. These values represent the extremes of the **CT** and **CL** solution space. Therefore, these two point values are set as the maximum and minimum values for $T$ and $L$ when normalizing, i.e., $T_{4C} = T_{min}$, $T_{0.5C} = T_{max}$, $L_{4C} = L_{max}$, $L_{0.5C} = L_{min}$. Subsequent adaptation value calculations will use these parameters.

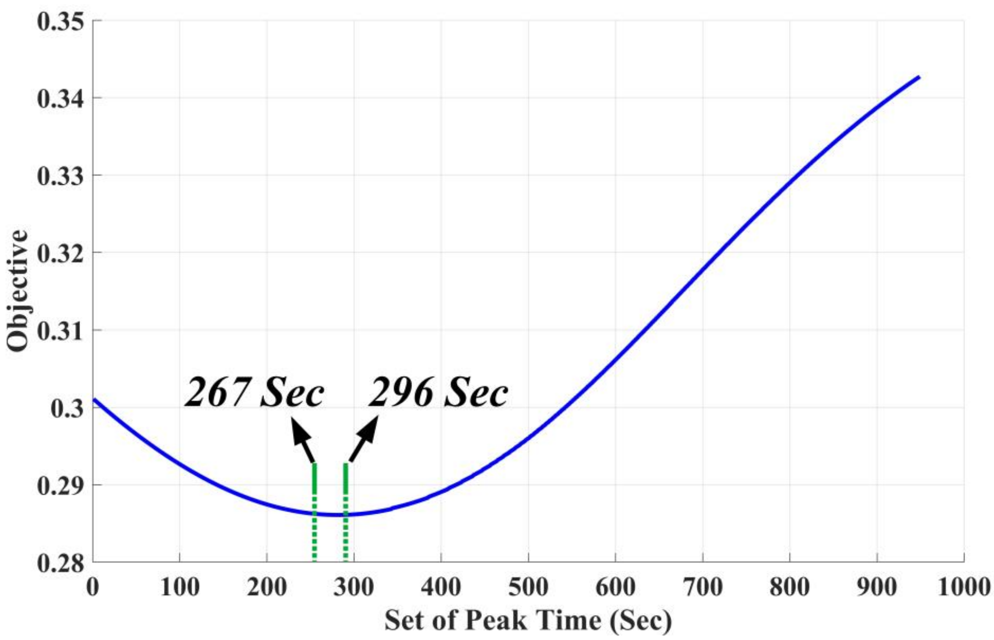


**Figure 17.** Fitness values for different transition times in basic CT-CV charging simulation.

**Table 4. CL** and **CT** for 0.5C and 4C CC-CV charging.

| C-Rate | CT (s) | CL (J) |
|---|---|---|
| 0.5 | 9062 | 566.2 |
| 4 | 3414 | 3540.5 |

### 4.3. Experimental Results

The comparison in this paper includes charging **TR**, charging efficiency, and **CT**. The proposed loss-minimization CT-CV charging method, the basic CT-CV charging method with the same transition temperature, and the CC-CV charging technique are compared. The following explains the experimental results.

#### 4.3.1. Comparison of Loss-Minimization CT-CV with Different Transition Times

This section compares the three optimized transition times, which are 267 s, 282 s, and 296 s, respectively. The PID parameters used in this experiment are $k_p$ = 8, $k_i$ = 0.005, and $k_d$ = 0.1. Figures 16 and 17 show the battery temperature waveform and charging current waveform for the three transition times of CT-CV charging. Table 4 compares the CT-CV charging effects for the three transition times. From Figures 18 and 19, and Table 5, it is observed that the 296 s transition time results in a larger maximum **TR** due to the extended 2C **CT**. On the other hand, the 267 s transition time results in a longer total **CT** due to the short 2C **CT**. By calculating the fitness value with the **CT** and **CL** for each set of parameters, it is determined that the 282 s transition time yields the lowest fitness value. Therefore, the 282 s transition time is considered the loss-minimization CT-CV charging method.

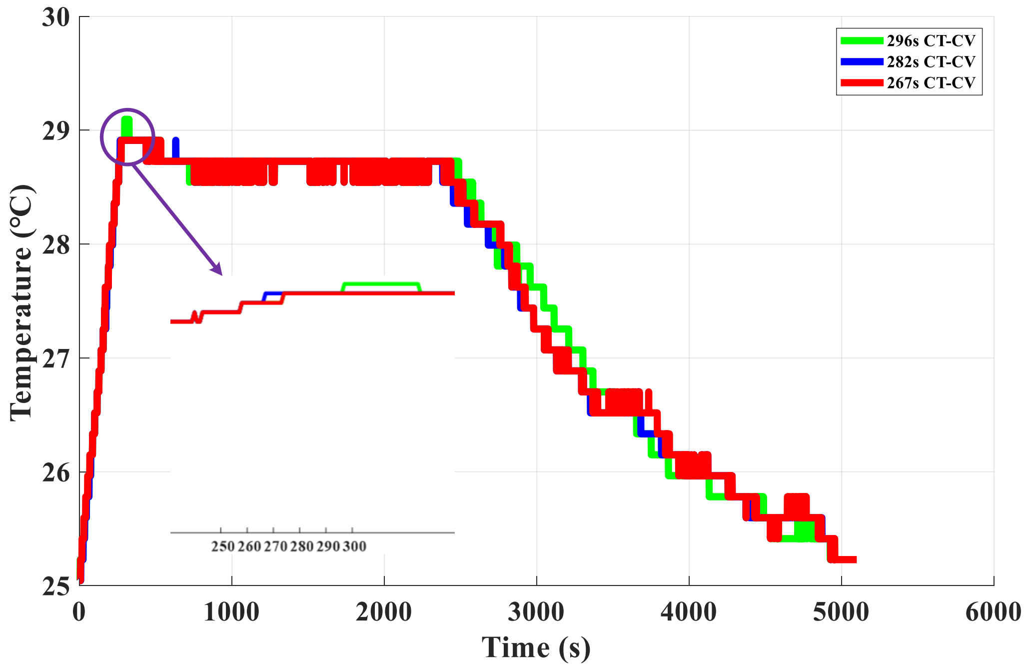


**Figure 18.** Battery temperature waveforms for three transition times in CT-CV charging method.

#### 4.3.2. Comparison of Different PID Parameters

Due to the Li-ion battery utilized in this paper, charging at 2C constant current for 282 s results in a battery temperature of 28.9 °C. Therefore, this section compares the performance of three types of PID value sets to maintain the battery temperature at 28.9 °C. The three sets of parameters are $k_p$ = 8, $k_i$ = 0.005, $k_d$ = 0.1; $k_p$ = 6, $k_i$ = 0.01, $k_d$ = 0.1; and $k_p$ = 4, $k_i$ = 0.015, $k_d$ = 0.1. Figures 18 and 19 show the battery temperature and charging current waveforms for each PID parameter set, and Table 6 compares their performance in stabilizing the battery temperature at 28.9 °C. Based on Figures 20 and 21 and Table 5, it is observed that the set of PID parameters $k_p$ = 8, $k_i$ = 0.005, and $k_d$ = 0.1 achieves the fastest stabilization at the set temperature with the least overshoot. Therefore, this set of PID parameters is used in all experiments in this study.

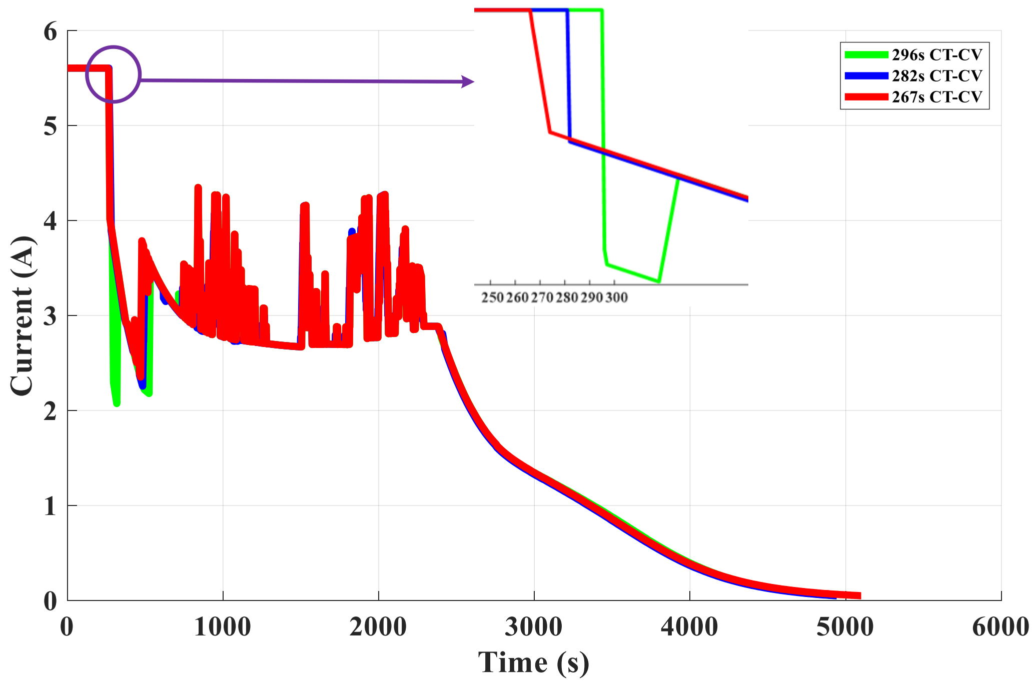


**Figure 19.** Charging current waveforms for three transition times in CT-CV charging method.

**Table 5.** Comparison of the charging effects for three transition times in CT-CV charging method.

| Transition Times (s) | CT (s) | Average TR (°C) | Max TR (°C) | Charging Efficiency (%) | Fitness |
|---|---|---|---|---|---|
| 267 | 5100 | 2.48 | 3.91 | 98.60 | 0.2551 |
| 282 | 4944 | 2.49 | 3.91 | 99.34 | 0.2535 |
| 296 | 4942 | 2.49 | 4.09 | 98.88 | 0.2547 |

Note: charging efficiency (%) = discharging capacity (mAh)/charging capacity (mAh).

**Table 6.** Comparison of three PID parameters to stabilize the battery at 28.9 °C.

| PID Parameter | Maximum Overshoot (°C) | Time Required for Temperature Stabilization (s) |
|---|---|---|
| $k_p = 8$, $k_i = 0.005$, $k_d = 0.1$ | 0.00 | 280 |
| $k_p = 6$, $k_i = 0.01$, $k_d = 0.1$ | 0.18 | 366 |
| $k_p = 4$, $k_i = 0.015$, $k_d = 0.1$ | 0.18 | 783 |

#### 4.3.3. Comparison between Loss-Minimization CT-CV and Various Cases

To ensure fairness in the comparison, this section compares the loss-minimization CT-CV charging method with the following methods: the basic CT-CV charging method with the same transition temperature of 28.9 °C, a 1.21C CC-CV charging method with an average temperature close to the loss-minimization CT-CV method, and a 1.40C CC-CV charging technique with **CT** close to the loss-minimization CT-CV charging technique. This comparison aims to validate the advantages of the proposed method. Figures 22–24 show the temperature, current, and voltage waveforms for each charging method, and Table 7 presents a comparison of these methods. According to Table 7, the loss-minimization CT-CV method has the lowest adaptation value. Compared with the fundamental CT-CV charging method with the same transition temperature of 28.9 °C, the proposed charging method increases the **CT** by 1.56% but reduces the average **TR** by 12.01% and the maximum TR by 24.81%. In comparison with the CC-CV charging technique with the same **CT**, it improves the average **TR** by 28.45% and the maximum **TR** by 27.46%. Compared with charging methods with the same average **TR**, it reduces the **CT** by 18.64% and the maximum TR by

19.05%. The improvement percentage, as indicated in Table 6, is calculated based on the proposed method in comparison to other charging methods.

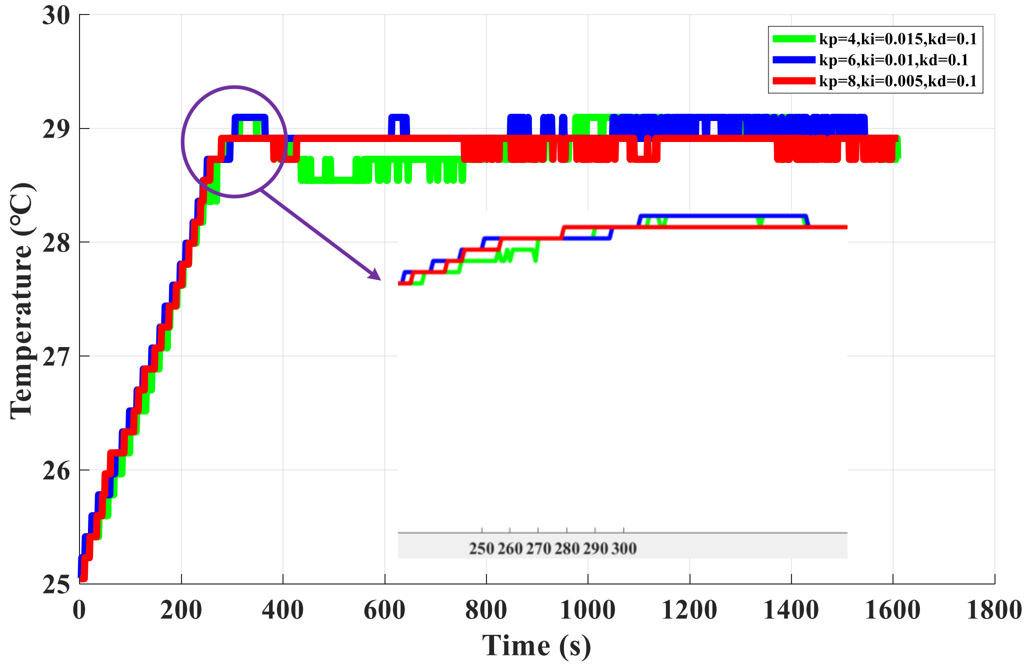


**Figure 20.** Battery temperature changes of three PID parameters.

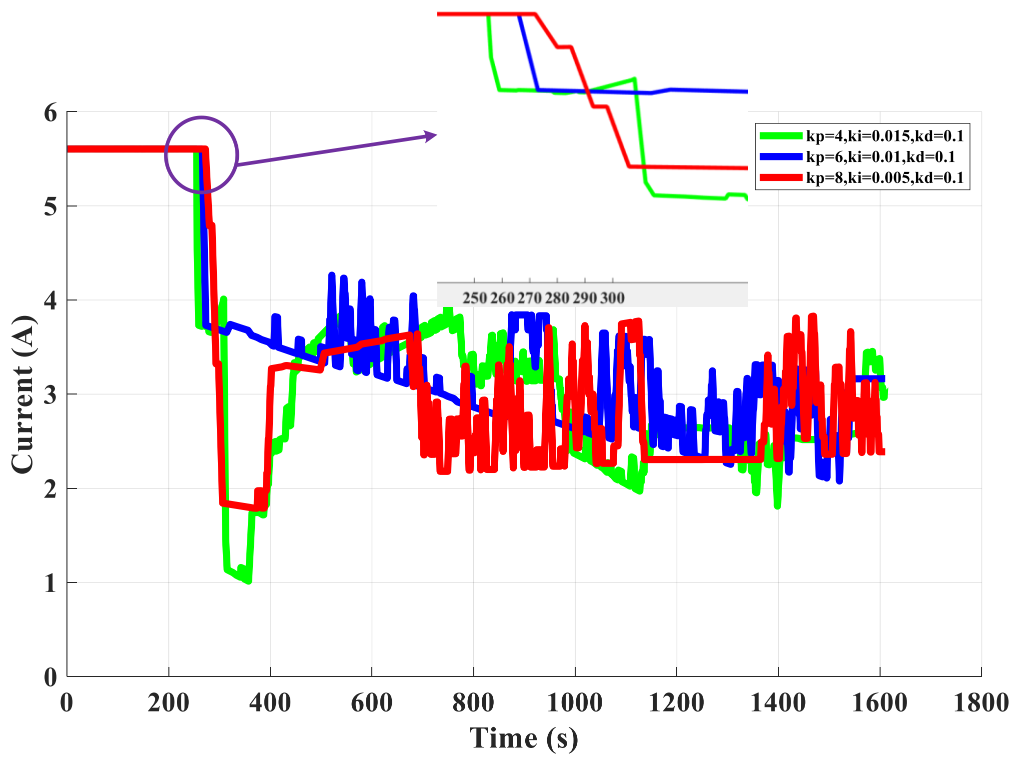


**Figure 21.** Charging current changes of three PID parameters.

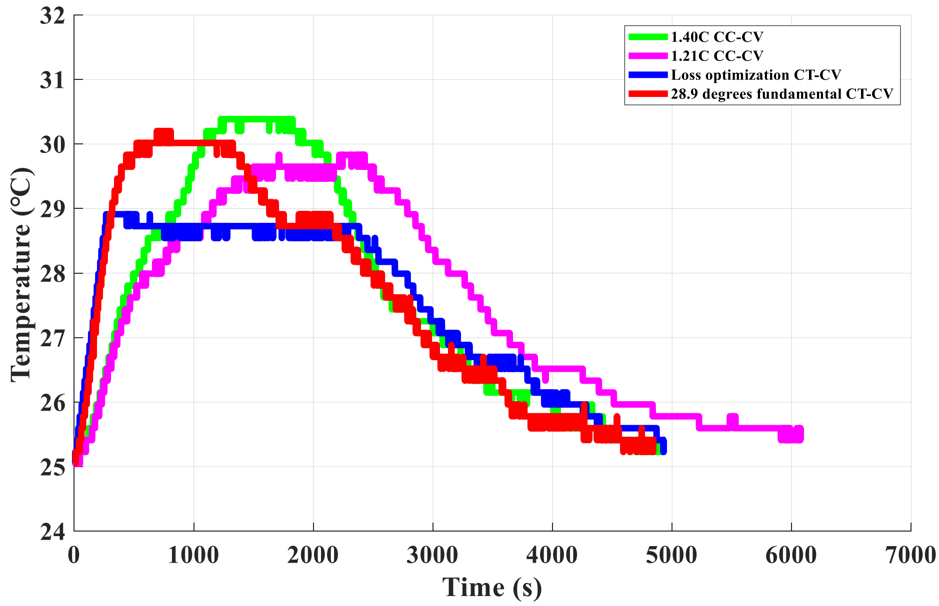


**Figure 22.** Battery temperature changes in each case.

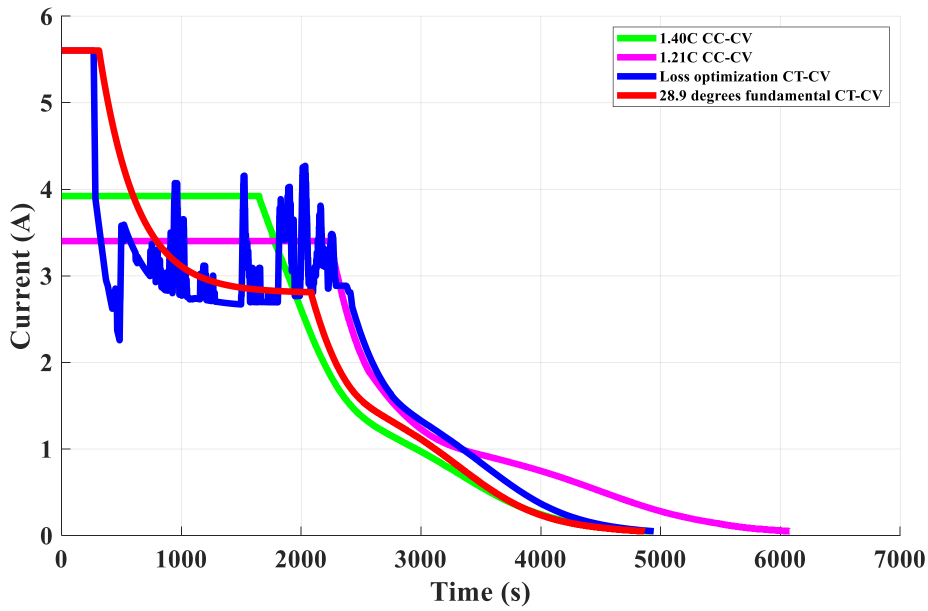


**Figure 23.** Charging current changes in each case.

**Table 7.** Comparison of charging methods.

| Charging Method | CT (s) | Average TR (°C) | Max TR (°C) | Charging Efficiency (%) | Fitness |
|---|---|---|---|---|---|
| Loss optimization CT-CV | 4944 | 2.49 | **3.91** | 99.34 | **0.2535** |
| 28.9 degrees fundamental CT-CV | 4868 (−1.56%) | 2.83 (+12.01%) | 5.20 (+24.81%) | 98.71 | 0.2638 |
| Same **CT** CC-CV (1.40C CC-CV) | 4926 (−0.37%) | 3.48 (+28.45%) | 5.39 (+27.46%) | 99.32 | 0.2828 |
| Same average **TR** CC-CV (1.21C CC-CV) | 6077 (+18.64%) | 2.49 (+0.00%) | 4.83 (+19.05%) | 99.48 | 0.3648 |

Note: charging efficiency (%) = discharging capacity (mAh)/charging capacity (mAh).

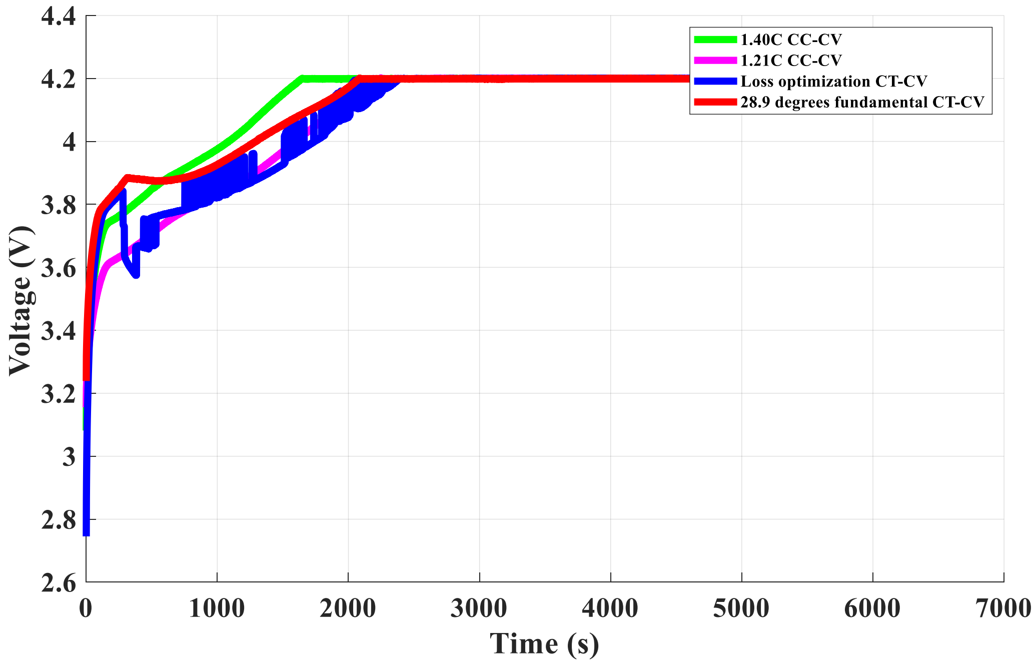


**Figure 24.** Battery voltage changes in each case.

## 5. Conclusions

This paper is based on the CT-CV charging method, utilizing the Coulomb counting method and the ECM of the battery to calculate the **CL** and **CT** for the CT-CV charging method. Using Matlab for the simulation involves assessing the charging losses and charging time resulting from CC-CV charging at rates ranging from 0.5C to 4C. Additionally, fitness evaluation is incorporated, utilizing the straight-line distance between two points as the score for the fitness value. Consequently, both objectives are simultaneously considered in searching for the transition point that minimizes losses, aiming to reduce **CT** while lowering the battery **TR**. The proposed charging method is applied to charge lithium-ion batteries to validate simulation results. Comparative analyses are conducted with the CT-CV charging method and the conventional CC-CV charging method. The results confirm the advantages of the proposed loss-minimizing CT-CV charging method in terms of shortened CT and reduced **TR** during charging. In comparison with the fundamental CT-CV charging method at 28.9 degrees Celsius, the proposed method increases CT by 1.56% but reduces average **TR** by 12.01% and maximum **TR** by 24.81%. Compared with the CC-CV charging method with the same **CT**, the proposed method reduces average TR by 28.45% and maximum **TR** by 27.46%. Furthermore, compared with the CC-CV charging method with the same average **TR**, the proposed method shortens CT by 18.64% and reduces maximum **TR** by 19.05%. Finally, the proposed method is verified to have the optimal fitness value by substituting the obtained **CT** and **CL** into the fitness calculation formula. It will be important for future research to investigate and establish an equivalent circuit model for a battery pack with multiple cells in series. Additionally, applying optimization methods to consider battery lifecycle and searching for the optimal PID parameters will be crucial.

From the experimental results, it is evident that the loss-minimizing CT-CV charging method proposed in this paper simultaneously considers reducing CL and shortening CT for lithium-ion battery charging. The method offers the following advantages:

1. This paper considers the equivalent impedance of the battery at different remaining capacities, enabling accurate estimation of **CL**.
2. The method identifies the optimal transition time.
3. It allows for the incorporation of other charging constraints for further optimization analysis.

**Author Contributions:** Conceptualization, G.-J.C. and Y.-H.L.; Methodology, G.-J.C. and Y.-H.L.; Software, J.-J.W.; Validation, Y.-H.L. and J.-J.W.; Formal analysis, C.-L.L. and J.-J.W.; Writing—original draft, G.-J.C., C.-L.L. and J.-J.W.; Writing—review & editing, G.-J.C.; Supervision, G.-J.C. and C.-L.L. All authors have read and agreed to the published version of the manuscript.

**Funding:** This research received no external funding.

**Data Availability Statement:** Data are contained within the article.

**Conflicts of Interest:** The authors declare no conflicts of interest.

## References

1. Hemavathi, S.; Shinisha, A. A study on trends and developments in electric vehicle charging technologies. *J. Energy Storage* **2022**, *52*, 105013. [CrossRef]
2. Jin, X. Aging-Aware optimal charging strategy for lithium-ion batteries: Considering aging status and electro-thermal-aging dynamics. *Electrochim. Acta* **2022**, *407*, 139651. [CrossRef]
3. Wassiliadis, N.; Schneider, J.; Frank, A.; Wildfeuer, L.; Lin, X.; Jossen, A.; Lienkamp, M. Review of fast charging strategies for lithium-ion battery systems and their applicability for battery electric vehicles. *J. Energy Storage* **2021**, *44*, 103306. [CrossRef]
4. Lin, Q.; Wang, J.; Xiong, R.; Shen, W.; He, H. Towards a smarter battery management system: A critical review on optimal charging methods of lithium ion batteries. *Energy* **2019**, *183*, 220–234. [CrossRef]
5. Shahjalal, M.; Roy, P.K.; Shams, T.; Fly, A.; Chowdhury, J.I.; Ahmed, M.R.; Liu, K. A review on second-life of Li-ion batteries: Prospects, challenges, and issues. *Energy* **2022**, *241*, 122881. [CrossRef]
6. Chen, L.-R. PLL-Based Battery Charge Circuit Topology. *IEEE Trans. Ind. Electron.* **2004**, *51*, 1344–1346. [CrossRef]
7. Chen, L.-R.; Chen, J.-J.; Chu, N.-Y.; Han, G.-Y. Current pumped battery charger. *IEEE Trans. Ind. Electron.* **2008**, *55*, 2483–2488.
8. Hsieh, G.-C.; Chen, L.-R.; Huang, K.-S. Fuzzy controlled Lithium-Ion Battery Charge System with Active State of Charge Controller. *IEEE Trans. Ind. Electron.* **2001**, *48*, 585–593. [CrossRef]
9. Liu, H.; Naqvi, I.H.; Li, F.; Liu, C.; Shafiei, N.; Li, Y.; Pecht, M. An analytical model for the CC-CV charge of Li-ion batteries with application to degradation analysis. *J. Energy Storage* **2020**, *29*, 101342. [CrossRef]
10. Chen, L.R.; Hsu, R.C.; Liu, C.S. A Design of A Grey-Predicted Lithium-Ion Battery Charge System. *IEEE Trans. Ind. Electron.* **2004**, *51*, 3692–3701.
11. Li, J.; Murphy, E.; Winnick, J.; Kohl, P.A. The Effects of Pulse Charging on Cycling Characteristics of Commercial Lithium-Ion Batteries. *J. Power Sources* **2001**, *102*, 302–309. [CrossRef]
12. De Jongh, P.E.; Notten, P.H.L. Effect of Current Pulses on Lithium Intercalation Batteries. *Solid State Ion.* **2002**, *148*, 259–268. [CrossRef]
13. Chen, L.-R. A design of an optimal battery pulse charge system by frequency-varied technique. *IEEE Trans. Ind. Electron.* **2007**, *54*, 398–405. [CrossRef]
14. Chen, L.-R. A design of Duty-Varied Voltage Pulse Charger for Improving Lithium-Ion Battery-Charging Response. *IEEE Trans. Ind. Electron.* **2009**, *56*, 480–487. [CrossRef]
15. Niroshana, S.I.; Sirisukprasert, S. Adaptive Pulse Charger For Li-Ion Batteries. In Proceedings of the 8th International Conference of Information and Communication Technology for Embedded Systems (IC-ICTES), Chonburi, Thailand, 7–9 May 2017.
16. Amanor-Boadu, J.M.; Guiseppi-Elie, A.; Sánchez-Sinencio, E. Search for Optimal Pulse Charging Parameters for Li-Ion Polymer Batteries Using Taguchi Orthogonal Arrays. *IEEE Trans. Ind. Electron.* **2018**, *65*, 8982–8992. [CrossRef]
17. Liu, Y.-H.; Hsieh, C.-H.; Luo, Y.-F. Search for an Optimal Five-Step Charging Pattern for Li-Ion Batteries Using Consecutive Orthogonal Arrays. *IEEE Trans. Energy Convers.* **2011**, *26*, 654–661. [CrossRef]
18. Liu, Y.-H.; Luo, Y.-F. Search for an optimal rapid charging pattern for Li-ion batteries using Taguchi approach. *IEEE Trans. Ind. Electron.* **2010**, *57*, 3963–3971. [CrossRef]
19. Vo, T.T.; Chen, X.; Shen, W.; Kapoor, A. New charging strategy for Li-ion batteries based on the integration of Taguchi method and state of charge estimation. *J. Power Sources* **2015**, *273*, 413–422. [CrossRef]
20. Liu, Y.-H.; Teng, J.-H.; Lin, Y.-C. Search for an optimal rapid charging pattern for Li-ion batteries using ant colony system algorithm. *IEEE Trans. Ind. Electron.* **2005**, *52*, 1328–1336. [CrossRef]
21. Wang, S.-C.; Liu, Y.-H. A PSO-based fuzzy-controlled searching for the optimal charge pattern of Li-ion batteries. *IEEE Trans. Ind. Electron.* **2015**, *62*, 2983–2993. [CrossRef]
22. Khan, A.B.; Choi, W. Optimal Charge Pattern for the High-Performance Multistage Constant Current Charge Method for the Li-Ion Batteries. *IEEE Trans. Energy Convers.* **2018**, *33*, 1132–1140. [CrossRef]
23. Dung, L.-R.; Yen, J.-H. ILP-based algorithm for Lithium-ion battery charging profile. In Proceedings of the 2010 IEEE International Symposium on Industrial Electronics, Bari, Italy, 4–7 July 2010.
24. Lee, C.-H.; Chang, T.-W.; Hsu, S.-H.; Jiang, J.-A. Taguchi-based PSO for searching an optimal four-stage charge pattern of Li-ion batteries. *J. Energy Storage* **2018**, *21*, 301–309. [CrossRef]
25. Lee, C.-H.; Chen, M.-Y.; Hsu, S.-H.; Jiang, J.-A. Implementation of an SOC-based four-stage constant current charger for Li-ion batteries. *J. Power Sources* **2018**, *18*, 528–537. [CrossRef]

26. Patnaik, L.; Praneeth, A.V.J.S.; Williamson, S.S. A Closed-Loop Constant-Temperature Constant-Voltage Charging Technique to Reduce Charge Time of Lithium-Ion Batteries. *IEEE Trans. Ind. Electron.* **2018**, *66*, 1059–1067. [CrossRef]
27. Molicel INR-18650-P28A Lithium Ion Battery Specification. Available online: https://www.molicel.com/wp-content/uploads/INR18650P28A-V1-80093.pdf (accessed on 15 July 2019).